Howard Hughes Medical Institute

Published as: *Nat Struct Mol Biol*. ; 18(10): 1172–1174.

Apo and $InsP_3$-bound crystal structures of the ligand-binding domain of an $InsP_3$ receptor

Chun-Chi Lin[1,2], **Kyuwon Baek**[1,2], and **Zhe Lu**[1]

[1]Department of Physiology, Howard Hughes Medical Institute, Perelman School of Medicine, University of Pennsylvania, Philadelphia, PA, 19104, USA

Abstract

We report the crystal structures of the ligand-binding domain (LBD) of a rat inositol 1,4,5-trisphosphate ($InsP_3$) receptor ($InsP_3R$) in its apo and $InsP_3$-bound conformations. Comparison of these two conformations reveals that LBD's first β-trefoil fold (β-TF1) and armadillo repeat fold (ARF) move together as a unit relative to its second β-trefoil fold (β-TF2). Whereas apo-LBD may spontaneously transition between gating conformations, $InsP_3$ binding shifts this equilibrium towards the active state.

Binding of $InsP_3$ to $InsP_3R$ in the endoplasmic reticulum (ER) membrane opens the Ca^{2+}-permeant pore in the receptor protein[1-4]. The resulting Ca^{2+} efflux from the ER elevates the cytoplasmic free Ca^{2+} concentration, a signal that triggers numerous important cellular processes[1, 3]. The LBD of $InsP_3R$, which comprises the ~600 amino-terminal residues[5, 6], is coupled to and thereby exerts allosteric control over the trans-membrane pore domain. Even when produced as an isolated construct, LBD binds $InsP_3$ with affinity and selectivity comparable to those of the whole $InsP_3R$ protein[7-9]. The LBD sequence encodes the two β-trefoil folds, β-TF1 and β-TF2, followed by an ARF[10, 11]. While the structural significance of the existence of two β-TF lobes in LBD has remained unknown, a construct comprising only β-TF2 and ARF (termed $InsP_3$-binding core) binds $InsP_3$ with even higher affinity than the entire LBD or the whole protein[12]. Hence, β-TF1 is viewed as a suppressor of $InsP_3$ binding. Additional studies suggest that β-TF1 not only helps stabilize LBD but also couples its conformational changes to the gate of the ion pore[9, 13, 14]. The crystal structures of β-TF1 alone and of β-TF2 plus ARF bound with $InsP_3$ have been solved separately[10, 11]. The latter structure reveals how $InsP_3$ is coordinated by various side-chains in the binding sites at the ARF - β-TF2 interface, and mutation of these side-chains weakens $InsP_3$ binding. Several low-resolution (24 – 40 Å) structures of $InsP_3R$ have also been obtained by cryo-electron microscopy[15-18]. Despite this remarkable progress, the fundamental question of how $InsP_3$ binding induces the gating conformational changes of LBD remains.

Correspondence should be addressed to Z.L. (zhelu@mail.med.upenn.edu).
[2]These authors contributed equally to this work.

Accession code. Protein Data Bank: The atomic coordinates and structure factors for $InsP_3$ ligand-binding domain structures have been deposited with accession code 3T8S.

Author Contributions: C-C. L., K.B. and Z.L. performed the experiments, analyzed the data, and prepared the manuscript.

To help address this question, we solved two LBD crystal structures of rat type 1 $InsP_3R$ (3.8 Å resolution; Fig. 1). Although the LBD crystal we used was grown in the presence of $InsP_3$, the two molecules in each asymmetric unit are in distinct conformations: one with and one without substantial $InsP_3$ occupancy. Diffraction data and structure refinement statistics are summarized in Supplementary Table 1, whereas LBD sequence and secondary structure assignments are shown in Supplementary Fig. 1. To illustrate the quality of the electron density map, we show a section of the 2Fo-Fc map and the corresponding structure in Fig. 2a.

The backbone structure of a given lobe of LBD in one state is largely superimposable upon that in the other state, or upon the previously determined structures of β-TF1 (PDB 1XZZ)[11] and of β-TF2 plus ARF (PDB 1N4K)[10] (Supplementary Fig. 2). In both LBD structures the C-terminal region 581-602 of ARF is disordered. The three lobes in LBD: β-TF1, β-TF2 and ARF, are arranged in a triangle (Fig. 1a, b). A similar triangular architecture is adopted by its counterpart in ryanodine receptors (RyR), the other type of intracellular Ca^{2+} release channel[19]. Given that, unlike its RyR counterpart, $InsP_3R$-LBD evolved to bind $InsP_3$, it is unsurprising that their structures differ in the lobes' relative orientation and within individual lobes (Supplementary Fig. 3).

As expected, $InsP_3$ binds between ARF and β-TF2[10]. To illustrate the difference in $InsP_3$ occupancy between the two $InsP_3R1$-LBD conformations, we show the relevant regions of an (Fo-Fc) $InsP_3$-omit map contoured at 4 σ and superimposed on the corresponding structures. The map was calculated using a model where neither molecule contains $InsP_3$ (Fig. 2b, c). For one molecule in the asymmetric unit (Fig. 2b), there is clear density at the site where $InsP_3$ is expected to bind on the basis of the previously solved structure of ARF and β-TF2 (PDB 1N4K) whereas for the other there is no visible density (Fig. 2c). Thus, the former molecule is primarily in an $InsP_3$-bound conformation and the latter in an unbound conformation. As expected, $InsP_3$-coordinating side-chains are disordered in the unbound structure.

The main global difference between LBD structures with and without $InsP_3$ bound is the relative orientation of the lobes (Fig. 1). To better illustrate this, we superimposed the two structures using the β-TF2 backbone as reference. In this alignment, ARF and β-TF1 undergo about a 10° rigid-body rotation (and slight translation) between the two states, such that ARF moves closer to β-TF2 to bind $InsP_3$ (Fig. 1c and 1d; Fig. 3a, b). This motion is more evident in a movie that alternates between the bound and unbound structures of LBD (Supplementary Movie 1). We also aligned bound and unbound structures of LBD, using the other trefoil fold (β-TF1) as reference. This second alignment reveals that the entire ARF plus β-TF1 portion of the two structures is largely superimposable between the two states (Fig. 3c) whereas the orientation of β-TF2 with respect to β-TF1 differs (Fig. 3d). This comparison reveals that the interface between the two β-TFs is dynamic, allowing them to undergo modest relative motion. The interface between ARF and β-TF2 is not only dynamic but also $InsP_3$ mediated. Given that the relative orientation of ARF and β-TF1 undergoes little change between bound and unbound states, the interface between them must be relatively static during that transition. The two linkers connecting the three lobes are in close proximity near one end of pseudo-three-fold axis (Fig. 1a, b). These linkers have previously

been suggested to be flexibile[14]. In the LBD structures, the linker joining the β-TFs consists of about ten residues and is sufficiently ordered to reveal the main-chain density (Supplementary Fig. 4). It appears to differ somewhat between bound and unbound states, where flexible Gly236 and Gly237 may facilitate the linker's motion (Fig. 1a, b; Supplementary Fig. 4). On the other hand, the linker between ARF and β-TF2, formed by only four residues (PVSP), differs little between the two states (Fig. 1a, b).

From a symmetry viewpoint, the following description offers a simple synopsis of LBD's overall architecture and how it transitions between the two observed states (Fig. 1; Supplementary Movie 1). The two β-TF lobes are similar (Fig. 1), except that β-TF1 has a prominent helix-turn-helix, arm-like motif (colored lime in a and b or blue in c and d). These two lobes form a pseudo-duplex and share a dynamic interface that allows modest relative rotational motion. Each β-TF lobe also interfaces with ARF. A significant breakdown of this pseudo-symmetry occurs at the interfaces between ARF and each of the two β-TFs. The interface between ARF and β-TF1 is relatively static in the two states and $InsP_3$ independent, whereas the interface between ARF and β-TF2 is dynamic and $InsP_3$ dependent. The former, static, interface ensures a largely concerted motion of ARF and β-TF1 whereas the latter confers $InsP_3$-regulated conformational changes upon LBD. The movement of ARF relative to β-TF2 renders the $InsP_3$-binding site between them either suited or unsuited for capturing $InsP_3$. Successful capture of an $InsP_3$ molecule then “locks” LBD in a bound state that favors opening of the ion pore. If β-TF1 indeed couples $InsP_3$-dependent conformational states of LBD to the gate[9, 13], it would cause the gate to open while the other lobe (β-TF2) of the duplex and ARF move closer together to capture an $InsP_3$ molecule. It then follows that the relatively static interface between β-TF1 and ARF would in turn couple two remote and functionally coordinated regions, the $InsP_3$-interacting region in ARF and the gate-coupling region in β-TF1, and thereby confer efficient allosteric regulation upon $InsP_3R$.

Regarding β-TF1's interaction with ARF, mutations of β-TF1 such as L30K, L32K and D34K in the β2-β3 loop and others in the β5-β6 loop are known to enhance $InsP_3$ binding to LBD[11] (Supplementary Fig. 5). However, neither the structure of β-TF1 nor that of ARF plus β-TF2 has yielded clues as to which regions of ARF or β-TF2 interact with the β2-β3 and β5-β6 loops of β-TF1[10, 11]. In our LBD structures, the β2-β3 and β5-β6 loops of β-TF1 extend toward helix α4 of ARF (Supplementary Fig. 5). The electron density map exhibits continuous densities extending from the two β-TF1 loops to the ARF helix. In light of a previous report that the D448N mutant does not express[20], we point out that the density between helix α4 of ARF and the β2-β3 loop of β-TF1 appears to correspond to the Asp448 side chain in the helix, which could be within hydrogen bond distance from the backbone amide group of Leu32 at the tip of the β2-β3 loop.

Interactions between ARF and β-TF1 evidently impact $InsP_3$ binding, as perturbing their interface or removing β-TF1 enhances $InsP_3$ binding[11, 12]. To gain further insight, using β-TF2 as reference, we aligned our two LBD structures with the $InsP_3$-bound (ARF - β-TF2) structure of Bosanac et al.[10] (PDB 1N4K). Compared to our $InsP_3$-bound structure, the ARF in their structure is further rotated with respect to our unbound structure (Fig. 3e; for clarity

β-TF1 and β-TF2 are removed). Given that their structure lacks the suppressor β-TF1and thus has a higher affinity for $InsP_3$, it most likely represents a more tightly bound state.

In the structure of ARF plus β-TF2 previously solved by Bosanac et al.[10] (PDB 1N4K), the Gly487-Pro502 region forms a hairpin motif that lies parallel to its neighboring helices α5 and α9. It may be noteworthy that in our LBD structures this hairpin motif in ARF, although not fully ordered, appears to point towards helix α4 that contains Asp97, Glu99, and Glu104 (supplementary Fig. 6). This structural feature and the previous finding[10] that mutation of these residues affects $InsP_3$ binding raise the issue of whether the ARF hairpin motif interacts with the arm motif of β-TF1.

In summary, the present crystal structures of LBD in both $InsP_3$-bound and -unbound conformations – two snapshots of the LBD dynamic process – provide the structural information necessary for uncovering the mechanism underlying allosteric regulation of $InsP_3R$. The two β-TFs of LBD form a pseudo-duplex with a dynamic interface that permits relative motion. The two lobes of this pseudo-duplex offer two separate interfaces to the ARF lobe as well. The interface between β-TF1 and ARF is relatively static so that these two lobes move largely together with respect to β-TF2. Such relative motion must in turn be coupled, presumably via β-TF1[9,13], to the ion-pore gate so that LBD exerts allosteric control over the gate. In contrast, the interface between β-TF2 and ARF is more dynamic and regulated by $InsP_3$. Given these characteristics, LBD, when not bound by $InsP_3$, would spontaneously transition between gating conformations but, when bound by $InsP_3$, would be locked in a state that favors opening of the ion pore.

Supplementary Material

Refer to Web version on PubMed Central for supplementary material.

Acknowledgments

We thank T.C. Südhof (Stanford University) for sharing the $InsP_3R1$-cDNA, J.K. Foskett (University of Pennsylvania) for providing the $InsP_3R1$-cDNA-containing plasmid and for discussion, K. Schmitz (University of Pennsylvania) for assistance in crystal diffraction, G. Van Duyne (University of Pennsylvania) for both the modified pET21 plasmid containing a TEV site and the TEV-cDNA-containing plasmid, staffs of the synchrotron beam lines at the Advanced Photon Source (GM/CA-CAT 23-ID-B and 23-ID-D) and the Advanced Light Source (8.2.1 and 8.2.2) for technical assistance, Y. Xu (University of Pennsylvania) for technical assistance, and P. De Weer (University of Pennsylvania) for critical review and discussion of our manuscript. This study was supported by the Howard Hughes Medical Institute.

References

1. Berridge MJ, Lipp P, Bootman MD. Nat Rev Mol Cell Biol. 2000; 1:11–21. [PubMed: 11413485]
2. Taylor CW, da Fonseca PC, Morris EP. Trends Biochem Sci. 2004; 29:210–219. [PubMed: 15082315]
3. Clapham DE. Calcium signaling. Cell. 2007; 131:1047–1058. [PubMed: 18083096]
4. Foskett JK, White C, Cheung KH, Mak DO. Physiol Rev. 2007; 87:593–658. [PubMed: 17429043]
5. Mignery GA, Sudhof TC. EMBO J. 1990; 9:3893–3898. [PubMed: 2174351]
6. Miyawaki A, et al. Proc Natl Acad Sci U S A. 1991; 88:4911–4915. [PubMed: 1647021]
7. Newton CL, Mignery GA, Sudhof TC. J Biol Chem. 1994; 269:28613–28619. [PubMed: 7961809]
8. Yoshikawa F, et al. Biochem Biophys Res Commun. 1999; 257:792–797. [PubMed: 10208862]

9. Rossi AM, et al. Nat Chem Biol. 2009; 5:631–639. [PubMed: 19668195]
10. Bosanac I, et al. Nature. 2002; 420:696–700. [PubMed: 12442173]
11. Bosanac I, et al. Mol Cell. 2005; 17:193–203. [PubMed: 15664189]
12. Yoshikawa F, et al. J Biol Chem. 1996; 271:18277–18284. [PubMed: 8663526]
13. Uchida K, Miyauchi H, Furuichi T, Michikawa T, Mikoshiba K. J Biol Chem. 2003; 278:16551–16560. [PubMed: 12621039]
14. Chan J, et al. J Mol Biol. 2007; 373:1269–1280. [PubMed: 17915250]
15. Jiang QX, Thrower EC, Chester DW, Ehrlich BE, Sigworth FJ. EMBO J. 2002; 21:3575–3581. [PubMed: 12110570]
16. Hamada K, Terauchi A, Mikoshiba K. J Biol Chem. 2003; 278:52881–52889. [PubMed: 14593123]
17. Serysheva II, et al. J Biol Chem. 2003; 278:21319–21322. [PubMed: 12714606]
18. Wolfram F, Morris E, Taylor CW. Biochem J. 2010; 428:483–489. [PubMed: 20377523]
19. Tung CC, Lobo PA, Kimlicka L, Van Petegem F. Nature. 2010; 468:585–588. [PubMed: 21048710]
20. Joseph SK, Brownell S, Khan MT. Cell Calcium. 2005; 38:539–546. [PubMed: 16198415]

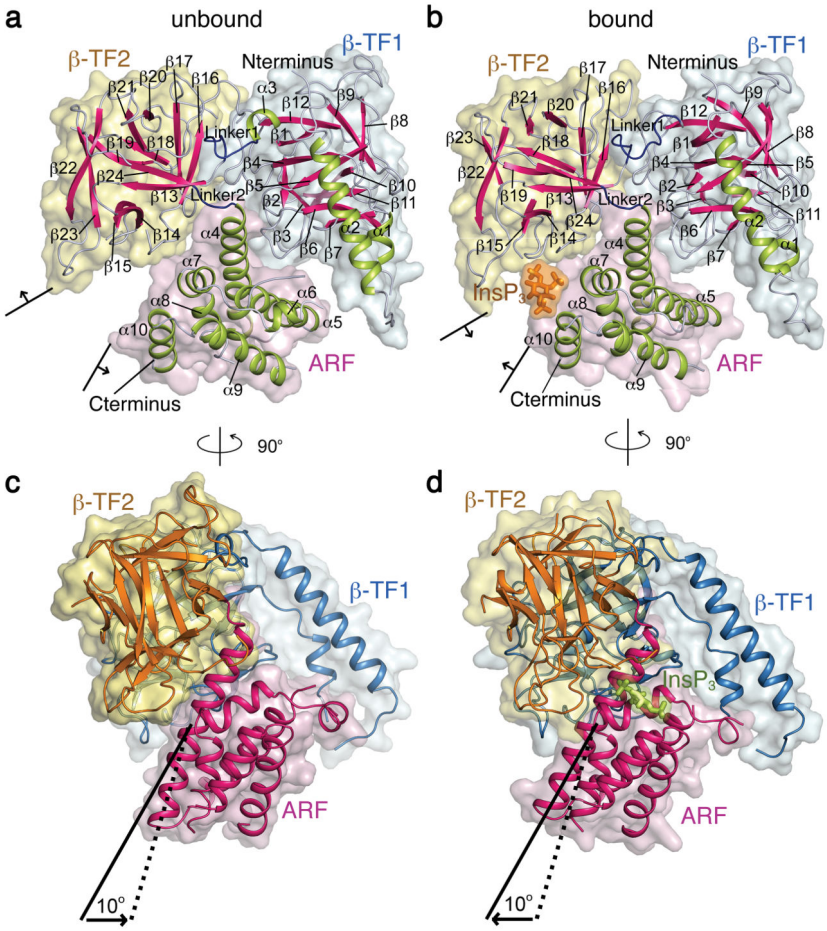

Figure 1.

Structures of LBD. (**a, b**) Surface and ribbon representations of LBD structures without (**a**) and with (**b**) $InsP_3$ bound, with β-TF2 shown in the same orientation. Surfaces of β-TF1, β-TF2, ARF, and $InsP_3$ are colored light blue, yellow, pink, and orange, respectively, whereas α helices, β strands, linkers between lobes, and the $InsP_3$ molecule are colored lime, magenta, blue and orange, respectively. (**c, d**) View of LBD structures rotated 90° from **a** and **b** where surfaces of the three lobes are colored as in a and b, and ribbon representations of β-TF1, β-TF2, and ARF are colored blue, orange and magenta, respectively. $InsP_3$ is shown in lime sticks. Solid and dotted lines indicate the axes of helix α4 in the bound and unbound states, respectively.

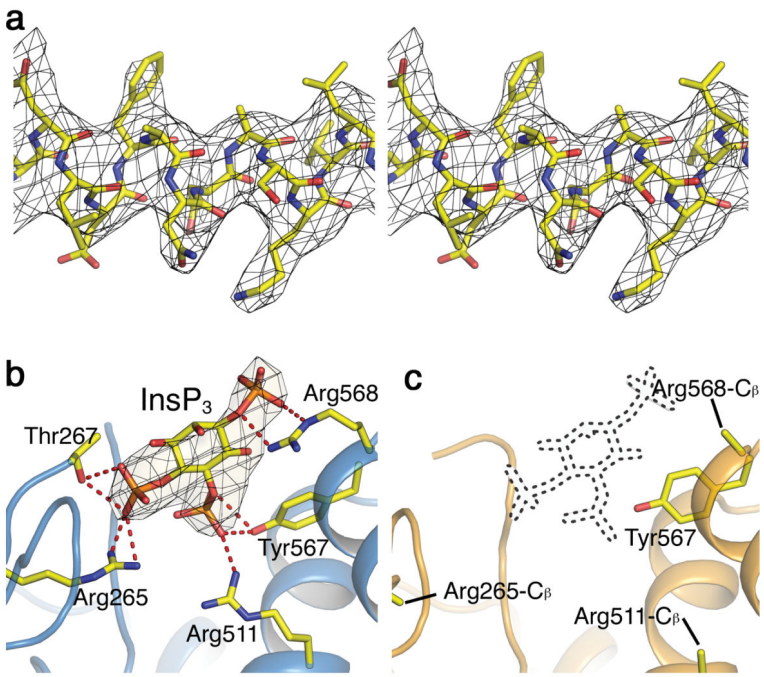

Figure 2.

Structures and electron density maps of regions within LDB. (**a**) Stereo view of a section (Asp442-Leu453) of helix α4 in the $InsP_3$-bound structure, superimposed on the corresponding 2Fo-Fc map contoured at 1 σ. (**b, c**) Structures of the $InsP_3$-binding site in LBD bound (**b**) or unbound (**c**) with $InsP_3$, superimposed on the respective Fo-Fc $InsP_3$-omit maps contoured at 4 σ. The $InsP_3$ molecule in panel **b** is shown as a stick model; the corresponding site in **c** is delineated by dots. The $InsP_3$-interacting side-chains, shown as sticks in **b**, are mostly disordered in **c**. The red dotted lines in **b** indicate potential hydrogen bonds.

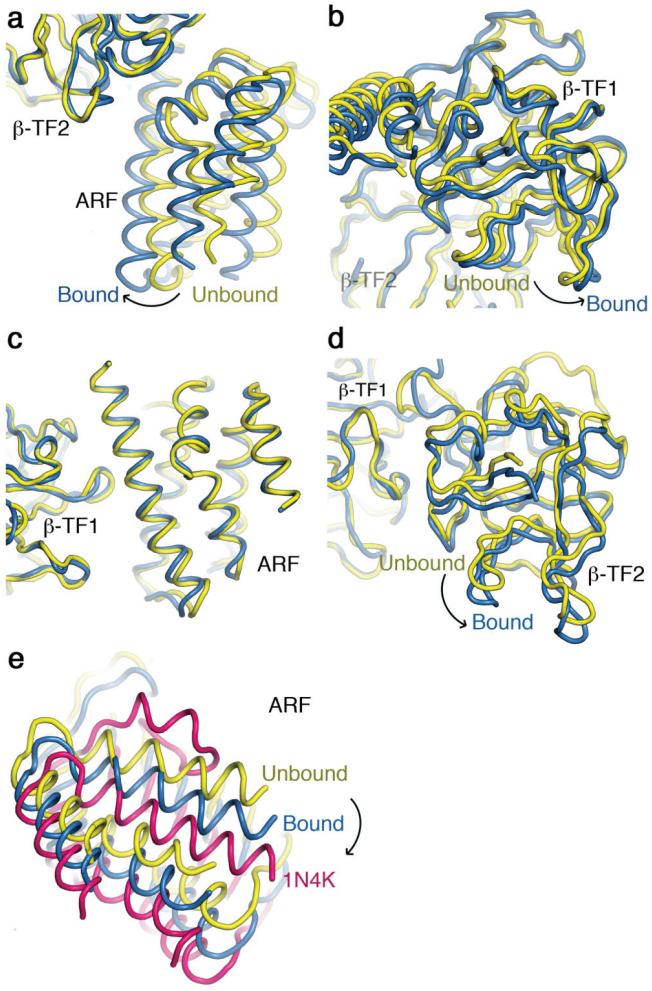

Figure 3.

Comparison of $InsP_3$-bound and -unbound LBD structures. (**a, b**) ARF (**a**) and β-TF1 (**b**) structures of bound (blue) and unbound (yellow) LBD are aligned using β-TF2 as a reference. (**c, d**) ARF (**c**) and β-TF2 (**d**) structures of bound (blue) and unbound (yellow) LBD are aligned using β-TF1 as a reference. (**e**) Shown are ARF structures of $InsP_3$-bound (blue) and -unbound (yellow) LBD as well as that of the $InsP_3$-bound partial LBD (magenta) (PDB 1N4K), all aligned using β-TF2 as reference. For clarity β-TF1 or β-TF2 or both are removed and, for easy comparison, the C-terminal 581-602 region of the partial LBD (PDB 1N4K) is not shown, as it is disordered in both LBD structures.